Can a Fish Learn to Ride a Bicycle? Sensorimotor Adaptation to Destabilizing Dynamics in Weakly Electric Fish

Yu Yang[1], Dominic G. Yared[2], and Noah J. Cowan[1,2,*]

[1]Department of Mechanical Engineering, Johns Hopkins University, Baltimore, MD, USA

[2]Laboratory for Computational Sensing and Robotics, Johns Hopkins University, Baltimore, MD, USA

[*]e-mail: ncowan@jhu.edu

1 Abstract

Animals (including humans) can readily learn to compensate for destabilizing dynamics, such as balancing an object or riding a bicycle, but it remains unclear how the nervous system learns to compensate for such destabilizing dynamics, and what the benefits of the newly learned control policies are. We examined how the weakly electric glass knifefish, *Eigenmannia virescens*, retunes its control system in the face of novel, destabilizing dynamics. Using a real-time feedback system, we measured fish swimming movements as they tracked a moving refuge, and fed the swimming movements back through novel dynamics to alter the motion of the very refuge they were tracking, creating an artificially destabilized reafferent loop. We discovered that fish learned to retune their sensorimotor controllers as the artificially destabilizing feedback was gradually introduced. This retuned controller reduced sensitivity of the sensorimotor system to low-frequency disturbances, such as would arise from turbulence or motor noise. When the artificial feedback was extinguished, fish exhibited a clear after effect, retaining their learned sensorimotor controllers for several minutes before washing out. This study sheds light on how the nervous system adapts to changing closed-loop dynamics and how those changes improve performance, and the after effects suggest a plasticity-based mechanism reminiscent of cerebellar learning.

2 Introduction

Animals routinely adapt to novel sensorimotor feedback. For example, insects can adjust to limb amputation [1–4], antenna trimming [5, 6], and wing damage [7–9] caused by predation or collisions. Humans are able to learn motor behaviors [10] like walking on split-belt treadmills [11, 12], counteracting visuomotor rotations and mirror reversal while tracking moving targets [13, 14], reaching for targets under artificially induced force-fields [15, 16], or riding a bicycle. Prior studies have revealed mechanisms and strategies of animals learning to compensate these effects in locomotion [1, 2]. However, from the perspective of control theory, it still remains unclear how animals learn novel dynamics and how the updated controllers impact system level performance. To address these questions, we studied well suited model organism, weakly electric glass knifefish *Eigenmannia virescens* refuge tracking system as a control loop and identified how the fish's sensorimotor controller changed under artificial, destabilizing feedback.

Eigenmannia virescens has been likened to an "aquatic hummingbird" [17], smoothly hovering in place or making agile movements to track a moving refuge [18]. These fish swim back and forth to sense their position within such a refuge [19–21], while also tracking the movements of the refuge [18,22,23]. These fore-aft swimming movements are produced by thrust forces generated by adjustments to the counter-propagating waves of its ribbon fin [24, 25]. *Eigenmannia* also relies on a robust feedback control system that is insensitive to the locomotor (plant) dynamics [25], and thus may not need to adapt to morphophysiological variability [25].

In this study, we examined sensorimotor adaptation in fish refuge tracking by designing an artificial feedback loop that could be used to alter the closed-loop dynamics; this experimental manipulation is analogous to inserting a dynamical system between the rotation of a steering wheel and the turning of the front wheels of a drive-by-wire automobile; in this way, the steering of the car could become non-intuitive and even unstable, if the driver failed to adapt their sensorimotor controller. Likewise, we increased gain in artificial feedback to destabilize the closed-loop refuge tracking system, systematically measuring each animal's sensorimotor controller along the way using system identification. Finally we removed the artificial feedback to assess any after effects—a hallmark of plasticity-based learning—in the sensorimotor controller.

3 Results

3.1 Fish tuned their controller dynamics in response to destabilizing feedback

We designed an artificial feedback loop to alter the closed-loop dynamics that fish experienced during refuge tracking (Figs. 1(A, B)). Specifically, we fed fish position back through a high-pass filter in real time and added it to a pre-defined pseudo-random sum-of-sines input (Fig. S1(A)) [14,23]. We increased the artificial feedback

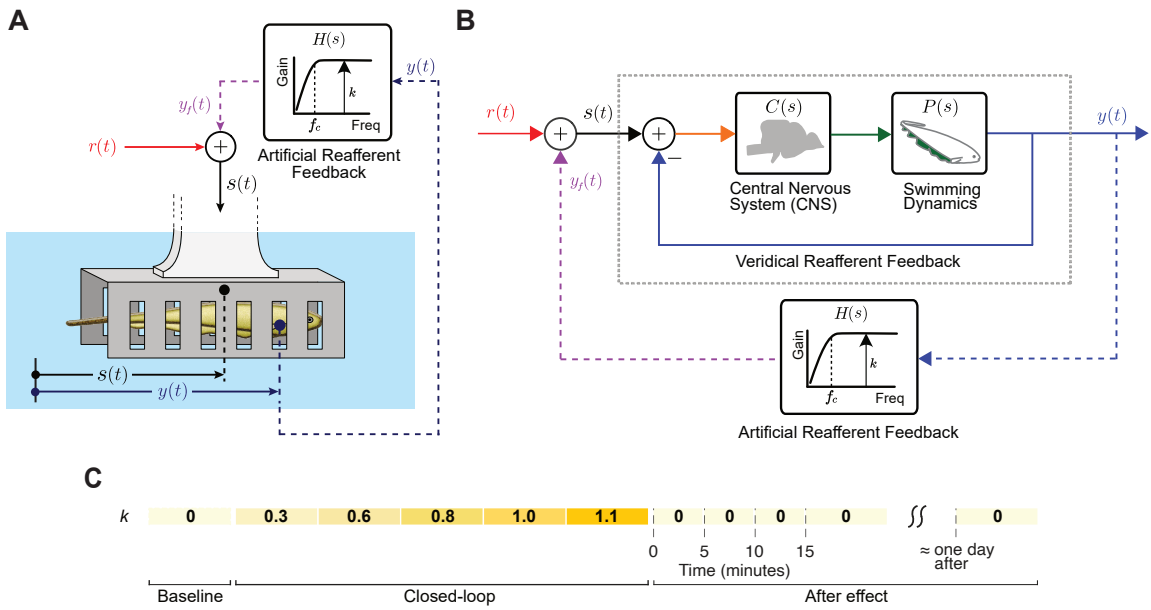

Figure 1. Experimental Protocol and Stimulus Design.
(A) Schematic of artificial, destabilizing feedback system. The longitudinal fish position, $y(t)$, was measured in real time using a custom video tracking system, and processed through a high-pass filter, $H(s)$ with gain k and cut-off frequency $f_c = 0.16$ Hz. The high-pass-filtered position, $y_f(t)$, was then added to a pseudo-random (sum-of-sines) reference signal $r(t)$, and fed to the refuge, i.e. $s(t) = y_f(t) + r(t)$, creating an artificial reafferent loop.
(B) Block diagram of the closed-loop system depicted in (A). The artificial, high-pass filter feedback is closed around the fish sensorimotor system (dotted black box). The fish is presumed to sense the difference between the longitudinal refuge position $s(t)$, and its own reafferent feedback $y(t)$. This difference is then processed by the nervous system, $C(s)$, and swimming dynamics, $P(s)$.
(C) Protocol: Experiments started from experimentally open-loop "baseline" phase ($k = 0$), followed by "closed-loop" phase in which we incrementally increased the artificial high-pass filter gain k from 0.3 to 1.1 over a course of about 33 minutes. Finally, we extinguished the artificial feedback to test for an "after effect" ($k = 0$ again). The sensorimotor controller was tested at five time intervals during the after effect phase: immediately after, 5 minutes, 10 minutes, 15 minutes and approximately one day after the end of "closed-loop" phase.

gain, k, on the high-pass filter incrementally in order to destabilize the closed-loop system (Fig. 1(C)). The experiments started from open-loop "baseline," followed by a "closed-loop" phase in which the high-pass feedback gain was gradually increased in discrete steps. This feedback was designed based on preliminary analysis [26] to destabilize the entire system in an effort to elicit learning. Finally, we removed the artificial feedback to assess after effects (see Materials and Methods, section 5.2).

To uncover how the artificial feedback changed fish's tracking response, we performed frequency domain system identification on $N = 7$ individuals (Materials and Methods) to estimate the empirical frequency response functions of individual fish; the frequency response functions we estimated comprises the fish's own reafferent feedback (see black dashed box in Fig. 1(B)), but does not include the artificial feedback. Using this method, we assessed how changes to the artificial feedback (via the gain k) led to changes in the fish's control system (as measured through its frequency response).

We found that fish systematically tuned their controllers under the artificial feedback. More specifically, as indicated in Fig. 2(A), fish added phase lead at intermediate frequencies (around 0.65 Hz) and increased sensorimotor gain, especially at higher frequencies (above 1 Hz) in response to the increasing artificial feedback gain k. This trend of increased gain and phase generalized across animals, as illustrated in Figs. 2(B, C).

3.2 Tuned controller reduced sensitivity to disturbances

The *sensitivity function* S (see Materials and Methods) reflects how well a feedback system suppresses disturbances [27], such as motor noise [28], turbulence [29], or other external forces. At frequencies ω for which $|S(j\omega)| < 1$ (improved *robustness*), the system *attenuates* disturbances. Conversely, the system *amplifies* disturbances when $|S(j\omega)| > 1$ (increased *fragility*) [27, 30]. Critically, for many systems, there is a tradeoff between "robustness" and "fragility" because of a general result, known as the "waterbed effect" [27], which states that the integral of the natural log of the sensitivity function magnitude—i.e., the *Bode sensitivity integral*—is 0:

$$\int_0^\infty \ln(|S(j\omega)|)d\omega = 0.$$

This result depends on technical details of system dynamics [27] (see Supplemental Materials Section 8.1 for details). This integral constraint produces a "conservation law," implying that suppressing disturbances ($\ln|S| < 0$, improving *robustness*) at some frequencies requires amplifying disturbances ($\ln|S| > 0$, increasing *fragility*) at other frequencies.

We computed the predicted sensitivity function for each feedback gain, k, based on each fish's baseline controller (estimated without the artificial, high-pass-filter feedback applied). This predicted sensitivity was

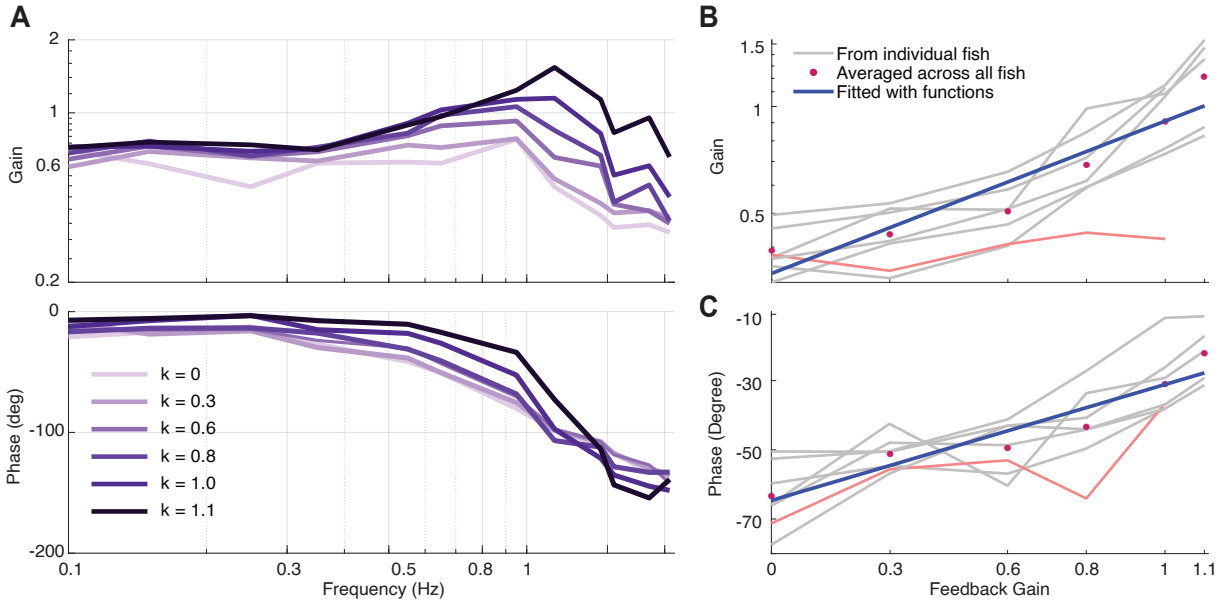

Figure 2. Fish Tuned Their Controller Dynamics in Response to Destabilizing Feedback. (A) Frequency response of one representative fish. As the feedback gain was increased, the gain of fish frequency response function increased (especially at frequencies > 0.95 Hz) and the phase lag decreased. (B) Gain of fish frequency response functions at 1.15 Hz and (C) phase at 0.65 Hz as a function of feedback gain k ($N = 7$ fish; data from two fish was excluded for $k = 1.1$ due to data quality). Linear functions (blue lines) were fitted to the averaged fish gains (pink dots) in logarithmic scale at 1.15 Hz and phases (pink dots) in linear scale at 0.65 Hz across all individual fish (gray curve)($p < 0.01$, Mann-Kendall test for trend for pooled data from $N = 7$ fish). All individuals exhibited positive correlation coefficients between high-pass gain k and log of gain at 1.15 Hz or phase at 0.65 Hz, and all correlations were significant ($p < 0.05$) except for one fish (red curve; same fish non-significant in both).

compared to the sensitivity function that the animal actually achieved when the feedback was applied. If the fish had not changed their controller, then the predicted and actual sensitivity functions would have been identical. For both the predicted and actual sensitivity functions, we approximated the bode integral over the experimental bandwidth of $0.1 - 2.05$ Hz ($0.63 - 12.9$ rad/s) using trapezoidal integration. Fig. 3(A) shows the natural logarithm of sensitivity function magnitude (predicted and actual) at $k = 1.1$ from one representative fish over this bandwidth; the Bode integral was approximated as the difference of the positive and negative areas of this function. Fig. 3(B) shows that, across fish, as the feedback gain k was increased, the Bode integral became increasingly negative compared to prediction ($p < 0.05$ for $k = 0.3$, $p < 0.01$ for each $k > 0.3$, paired-sample t test). This indicates that the change of fish controller brought about a benefit, i.e. reducing sensitivity to disturbances within this relatively low frequency band (< 2.05 Hz). Moreover, this enhancement over prediction became more pronounced with ever-increasing artificial feedback gains, as the difference between actual and predicted Bode integral decreased with increased gain k ($p < 0.05$,

Mann-Kendall test for the average across $N = 7$ fish, Sen's slope is around -0.16). Such tuned, low-frequency disturbance rejection may help suppress turbulence and other environmental and neuromuscular perturbations (see Discussion).

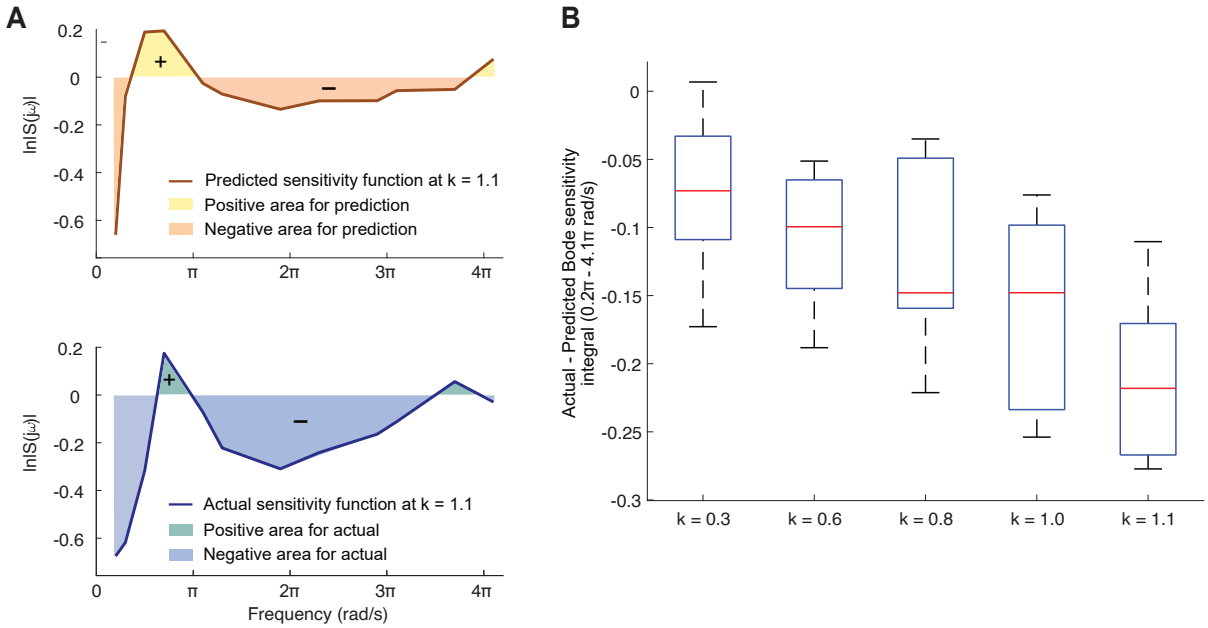

Figure 3. Tuned controller reduced sensitivity to disturbances.
(A) Predicted (based on baseline controller) and actual (based on fish's tuned controller) bode sensitivity functions for $k = 1.1$, from one representative fish. Here, the positive and negative areas are marked in different colors (see legend) and the natural logarithmic magnitude of actual bode sensitivity function has larger negative region compared with prediction. (See Supplemental Fig. S2 for larger frequency range.)
(B) For each individual, and at each gain k, we computed the differences between the actual and predicted Bode sensitivy integrals over the frequency range 0.2π–4.1π rad/s. Box and Whisker plots of these values are shown for all $N = 7$ individuals. The mean value across individuals was < 0 for each gain ($p < 0.05$ for $k = 0.3$, $p < 0.01$ for the remaining gains, paired-sample t test).

3.3 Fish maintained their learned controller, exhibiting clear after effect

We tested if after effects persisted when the closed-loop feedback was abruptly removed, as such after effects would indicate a plasticity-based mechanism, reminiscent of cerebellar learning [11, 12, 14]. We averaged the frequency responses in blocks of three or five trials during the "after effect" phase (see Fig. 1(C)), and compared the result with the "baseline" frequency response. Fig. 4(A) shows the averaged fish frequency response during the "after effect" phase, as well as the baseline phase, from one representative fish. In each frequency response plot, the fish was under normal, veridical feedback, with no artificial high-pass filter in the feedback loop. Note that just after the artificial feedback was removed, the frequency response gain and phases remained elevated, revealing that the tuned controller persisted for some time after the feedback was removed. Then, over time, the frequency responses returned to baseline, as the learned controller was

washed out.

To test whether this after effect was significant, we bootstrapped data across fish (Fig. 4(B)), and found that the averaged gain at 0.95 Hz of the first 20 seconds of the just-after phase was lower than the averaged gain in closed-loop ($k = 1.1$), but still remained significantly elevated above baseline. The frequency response gain then gradually decayed toward baseline phase within about 15 minutes. Similar trends were found in gain at 1.15 Hz and phase at 0.65 Hz (Fig. S3).

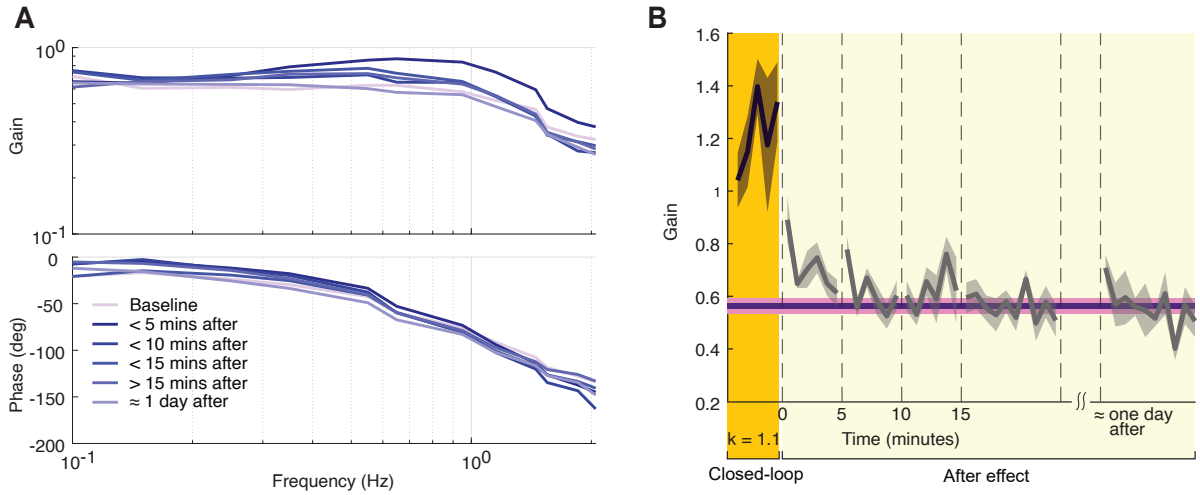

Figure 4. Fish maintained learned transfer function in "After effect" phase.
(A) Averaged fish frequency response from "baseline," "just after," "5 minutes after," "10 minutes after," "15 minutes after" and "≈ one day after" cases from online tracking data by one sampled fish. The frequency response gain and phases of the averaged "just after" case remained elevated.
(B) Fish frequency response gain at 0.95 Hz from late learning "$k = 1.1$" (when $t < 0$), "just after," "5 minutes after," "10 minutes after," "15 minutes after," and "≈ one day after" cases, by bootstrapping online tracking data (10000 times) across $N = 6$ fish. the gray solid lines are means and shaded regions are standard deviations (stds). The purple solid line is the mean of bootstrapped data in "baseline," while shaded region is std.

4 Discussion

We examined how animals adapted their controllers in the face of destabilizing, closed-loop dynamics. Fish clearly tuned their controller to enhance disturbance rejection, and the learned controller was retained after the destabilizing feedback was removed, suggesting a cerebellar or cerebellar-like adaptation process.

The tuned controller reduced the impact of disturbances, such as motor noise and turbulence. Such disturbances can take a variety of forms in biological systems. For example, humans can robustly reject mechanical disturbances to their hand during reaching [31]. Likewise, when a hawkmoth hovers in a flower's wake in windy environments, vortices are shed, perturbing the hawkmoth as it feeds from the swaying

flower [32]. Future field work could shed light on the relation between closed-loop disturbance rejection, its sensorimotor adaptation, and the natural statistics of environmental perturbations; this is similar to the work of Sponberg et al. [33], which examined the relation between closed-loop tracking performance of hawkmoths and the natural movement frequencies of flowers.

This paper focuses on learning of the feedback pathway, but learning can occur in both feedforward and feedback pathways. Kasuga et al. [34] discovered that feedforward adaptation and feedback adaptation were separately learned when human participants were trained to reach to two lateral and one central target with mirror-reversed visual feedback. Yang et al. [14] examined adaptation and *de novo* learning in visuomotor rotation and mirror-reversal tasks, suggesting that there could be two different control pathways, and that the mechanisms of learning in those pathways may be different. In general, feedforward control focuses on enhancing tracking and stimulus prediction (inverse internal model), while feedback control focuses on stability and disturbance rejection (forward model). Feedback adaptation involves learning rich feedback dynamics necessary for stability and performance. Future work could begin to put together these two control elements—feedforward and feedback control—to understand how are learned in tandem to improve sensorimotor performance in the face of novel dynamics—like riding a bicycle, balancing a pole, and juggling.

5 Material and Methods

Adult weakly electric glass knifefish *Eigenmannia virescens* (length: 10 – 15 cm) were obtained from commercial vendors and housed following the guidelines [35]. Temperature and conductivity of water in experimental aquarium were kept in a range of 76 °F – 80 °F and 10 μS/cm – 150 μS/cm, respectively. All fishes were transferred to the experimental aquarium 12 – 24 hours before the start of experiments. The experiments were conducted in illuminance level around 80 lux. All the experimental procedures were approved by the Johns Hopkins Animal Care and Use Committee and followed guidelines established by the National Research Council and the Society for Neuroscience.

5.1 Experimental Apparatus

The experimental apparatus was modified from the system described in [19]. The system uses a real-time measurement of the fish position, and feeds it back to the input. The system was modified in two ways: it now filters the fish position through a high pass filter before feeding it back to the input and it adds the feedback signal to a pre-designed sum of sines signal [26]. We refer to the high-pass-filtered feedback as "artificial reafferent feedback."

5.2 Experimental Protocol

We intended to drive the entire closed-loop system towards instability by increasing the gain in artificial feedback, and test whether there were after effects after turning the artificial feedback off.

Each experiment comprised three phases: "baseline," "closed-loop," and "after effect." Both "baseline" and "after effect" phases were open-loop (no high-pass-filter feedback).

In the "baseline" phase, we conducted five 60-second trials, with a 20-second rest period between each individual trial. The input stimulus in each trial comprised a 10 seconds ramp-up, 40 seconds of sum-of-sines inputs, and 10 seconds ramp-down (see Fig. S1A). Functions are described in section 5.2.1. There were no pre-designed inputs during rest periods.

In the "closed-loop" phase, a first order high-pass filter was in the artificial feedback loop. The high-pass filter gain k was increased incrementally: 0.3, 0.6, 0.8, 1.0, and 1.1 (Fig. 1C). Each feedback case was composed of five trials (60 seconds) with four rest period (20 seconds) in between. Critically, artificial feedback remained enabled during the rest periods in each feedback case. There were also 20 second rest periods connecting the last trial of each feedback case to the first trial in the next feedback case. During these periods, the feedback gain was linearly increased as a function of time from the last value of k to the next value. And during all rest periods in the "closed-loop" phase, there were no pre-defined reference inputs.

At the start of the "after effect" phase, the artificial feedback was extinguished. Experiments were conducted based on 5 time intervals after the end of closed-loop experiments: "just after," "5 minutes after," "10 minutes after," "15 minutes after," and "≈ one day after." The input stimulus, number of trials, and the duration of rest periods were the same as those in "baseline" phase. Three trials were collected for "just after," "5 minutes after" and "10 minutes after" cases.

5.2.1 Stimulus Design

The pre-designed reference signal has three phases: "ramp-up," "sum-of-sines," and "ramp-down," illustrated in Fig. S1A. In "ramp-up" and "ramp-down" phases, the designed signal oscillated at 0.45 Hz with modulated amplitude and was added to modulated sum of sines signal (Fig. S1A). The sum of 12 single sinusoidal functions, $r_1(t)$, is given (in centimeters) as follows:

$$r_1(t) = 0.8 \sum_{i=1}^{12} \frac{1}{2\pi 0.05 k_i} \cdot \cos(2\pi 0.05 k_i t + \Phi_i). \tag{1}$$

Here, $k_i = 2, 3, 5, 7, 11, 13, 19, 23, 29, 31, 37, 41$ are prime numbers and phase of each single sine component Φ_i is randomized. This creates a pseudo-random, unpredictable stimulus suitable for system identification [23].

5.3 Data Analysis

5.3.1 Online and Offline Tracking

Both the refuge position and fish position were measured in real time by a template matching based tracker in LabVIEW [19]. Sampling rate of the system was 25 FPS and online tracking data was saved in .csv files. Refuge tracking videos from each phase of the experiments were also saved as .mp4 files. To avoid apparatus latencies impacts on the accuracy of estimating the frequency response of fish in each feedback case, we individually tracked the fish and refuge motion on each video with offline tracking software DeepLabCut [36]. To improve efficiency, we combined videos across individuals when labeling frames and used those for network training (ResNet152 with 10000 iterations). Although most of the data were generated from that, for some fish, we separately labeled the frames from their own videos and trained the network specifically for them to obtain a better result. The choice of network or number of iterations might be different from the combined one. All offline data was finally saved in .csv files with the 2-D position of refuge and fish, together with the likelihood of each data point.

5.3.2 System Identification

After obtaining the refuge and fish position in time domain, we performed system identification with $N = 7$ fish. Most of the procedure for system identification follows the steps of sum-of-sines based system identification in [37]. For each phase (baseline, closed-loop, and after effect), we picked up the middle 40-second sum of sines part in each trial and divided them into two halves. We then transferred each 20 second input and output data into the frequency domain using the discrete Fourier transform (DFT). We then used the empirical transfer function estimate (ETFE) to estimate the Frequency Response Function (FRF) for each trial. Trials with tracking loss were discarded. Data from two fish were excluded for $k = 1.1$ due to large number of trials with tracking loss. The FRFs from each 20s segment were averaged to obtain a single estimate.

5.3.3 Bode Sensitivity Integral

The sensitivity function is defined as follows:

$$S(s) = \frac{1}{1 + C(s)P(s) - C(s)P(s)D(s)H(s)}, \tag{2}$$

where $s = j\omega$, $j = \sqrt{-1}$,

$$H(s) = \frac{ks}{s+1}, \tag{3}$$

is first order high-pass filter, and $D(s)$ is the system delay in forward loop (see Supplementary Material section 8.2). The multiplication of transfer function of "controller," i.e. $C(s)$, and that of "plant," i.e. $P(s)$, could be computed from estimated fish's FRFs by opening fish's reafferent feedback loop. The transfer function in artificial feedback was known, so the sensitivity function was then computed. To calculate the Bode sensitivity intergal over the frequency range $0.2\pi - 4.1\pi$ rad/s, we subtracted positive and negative trapezoidal regions formed by natural log of sensitivity function magnitude and x axis (Fig. 3).

5.3.4 Bootstrapping Analysis of After Effect

One of the most important questions of this research is whether the closed-loop novel dynamics have after effect on fish tracking behavior. To check this we analyzed online tracking data from ($N = 6$) fish. Note that the 7th fish was excluded due to failure in data collection. Here, for each 20-second replicate in "just after," "5 minutes after," "10 minutes after," "15 minutes after," and "$\approx$ one day after" cases, we performed bootstrapping ($n_{\text{boot}} = 10000$) across $N = 6$ fish in time domain. Then, we estimated the FRFs of 10000 bootstrapped time domain data. We excluded those when any tracking loss happened in any replicates from any fish. The mean and standard deviation (std) of 10000 bootstrapped FRFs were then computed for each replicate. Specifically, we also followed the same procedure to compute mean and std of bootstrapped FRFs in "baseline" and "closed-loop ($k = 1.1$)" cases so that we could compare those with bootstrapped FRFs in after effect cases.

6 Author Contributions

YY: Co-designed the experiments, performed the experiments, processed and analyzed data, wrote the original draft; DGY: Co-designed the experiments, performed the experiments, processed and analyzed data; NJC: Introduced the project idea, co-designed the experiments, oversaw data analysis, supervised the project, wrote the original draft, funding.

7 Acknowledgments

We thank B. Vágvölgyi for modifying the experimental system for the experiments, L. N. Peterson and H. Yeh for data collection and analysis, and E. S. Fortune, C. S. Yang, D. Biswas and D. Cao for helpful discussions. We thank K. T. Yoshida, I. Uyanik, and E. E. Sutton for pilot experiments.

8 Supplemental Materials

8.1 A More General Results of Bode Sensitivity Integral

Our results introduced "waterbed effect", where the system suppresses the disturbances at some frequencies at the cost of enhancing disturbances at other frequencies because Bode sensitivity integral equals zero. However, that result requires certain conditions of system dynamics. A more general result of Bode sensitivity integral is given here [38]:

$$\int_0^\infty \ln(|S(j\omega)|)d\omega = \pi \sum_{k=1}^{m} \mathrm{Re}(p_k) - \frac{\pi}{2} \lim_{s\to\infty} sL(s),$$

where p_k $(k = 1, 2, \ldots, m)$ are the unstable right half plane poles of the *loop function* $L(s)$ of the system. The relationship between *loop function* and *sensitivity function* of the same system is:

$$S(s) = \frac{1}{1 + L(s)}.$$

Thus, when *loop function* L of the feedback system satisfies the following two conditions: 1) has no unstable poles and 2) converges to 0 faster than $1/s$ as $s \to \infty$ (in other words, has at least two more poles than zeros), the Bode sensitivity integral is 0. However, we could not directly determine if these conditions were satisfied by just looking at our data, because our stimulus only included low frequencies between 0.2π rad/s and 4.1π rad/s which were more relevant to fish's bandwidth. Therefore, we fitted fish controller times plant $C(s)P(s)$ data with a "canonical second order model with delay" [37]:

$$C(s)P(s) = \frac{A{\omega_n}^2}{s^2 + 2\zeta\omega_n s + {\omega_n}^2} e^{-\tau_d s}.$$

This model of CP fits data well (see Fig. S2). And the computed $L = CP - CPDH$ from it satisfies the above two conditions for Bode sensitivity integral to be 0. Also, the model extrapolated sensitivity function S at higher frequencies (above 4.1π rad/s) and $\ln(|S|) > 0$ at frequency band around $2\pi \times 2 - 2\pi \times 5$ rad/s (Fig. S2(A)) well illustrated "waterbed effect". Irrespective of that, results from data could only indicate that the tuned controller of fish helped surpresses disturbances over the frequency range $0.2\pi - 4.1\pi$ rad/s.

8.2 System Delay Analysis

The latencies in experimental setup can impact the accuracy of estimated fish's FRF in system identification, thus needs to be taken into consideration. In our system, the delay is mainly from latencies between reading

reference files from PC and triggering the linear actuator to control the refuge movement. We also did analysis and it turned out that other factors such as asynchronously saving the video and .csv file and artificial feedback processing delay from FPGA are negligible.

In control theory, delay could easily be modeled by transfer function $e^{\tau s}$, where τ is time constant. Here we denote the system delay as $D(s)$. We processed the videos recorded during experiments with tracking software DeepLabCut [36] to generate the offline refuge movement, and estimated the delay in frequency domain by taking the ratio of Fourier domain offline refuge trajectories and Fourier domain online refuge trajectories saved from experimental setup.

9 Appendix

9.1 Disturbances in Fish Refuge Tracking Task

Sefati et al. [24] indicated that the fore-aft movement of fish relies on mutually opposing thrust forces generated by two inward-counter-propagating waves of its ribbon fin. The change of thrust forces is linearly controlled by fish adjusting where these two waves meet (i.e. "nodal point" position). They also found a damping force opposing the direction of velocity of fish during tracking. That force arose from asymmetries in net velocities of the counter-propagating waves caused by body fore-aft velocity [24]. Based on these findings, Sefati et al. [24] constructed a simple lumped-parameter task level dynamical model for the "plant" of fish:

$$m\ddot{x} + \beta\dot{x} = F, \tag{4}$$

where m is the mass of fish, β is the damping constant, F is the net thrust force generated by nodal point movement of ribbon fin, x, $\dot{x}$, $\ddot{x}$ are the position, velocity, and acceleration of fish in longitude direction, respectively. Uyanik et al. [25] quantified the nodal point position u (proportional to F in equation 4 with a nodal shift gain κ) as fish's motor output (input of the plant) and longitudinally position of fish x as system output, i.e.

$$F = \kappa u. \tag{5}$$

From control theory [27] we know that disturbance of a control system is added to the control input (i.e. motor output in biological system [39]) and the addition becomes input of the plant. As fish moving back and forth to track the refuge, it causes water turbulence in the tank as well. That could generate a disturbance force F_t impacting the longitudinally net force in fish tracking. Besides, the motor command noise d_m could

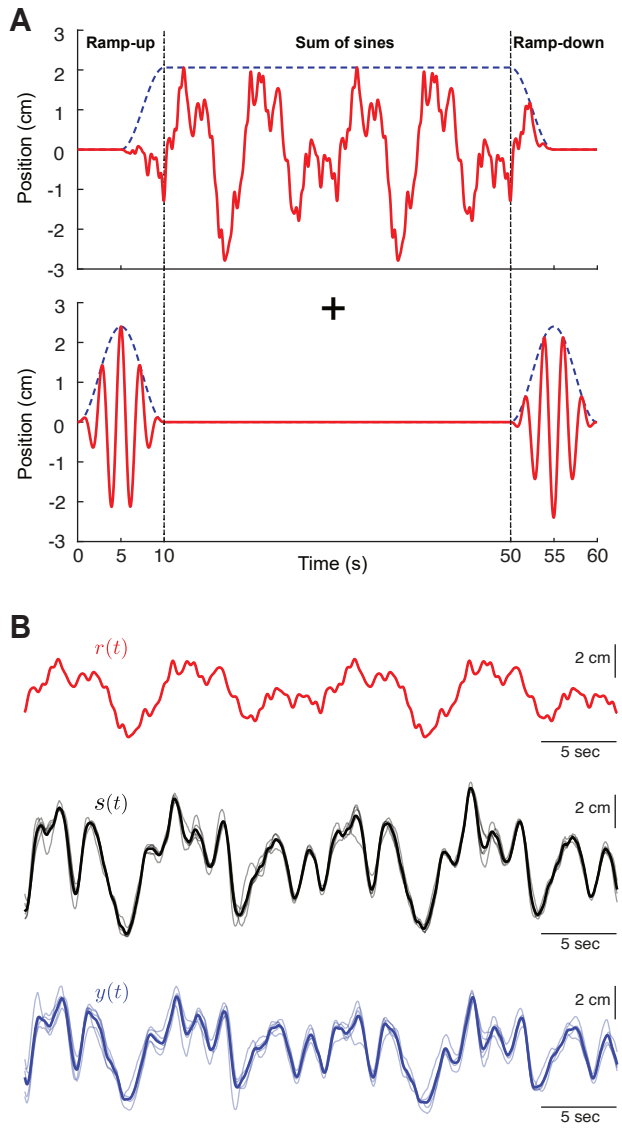

Figure S1. (A) Pre-designed Reference Signal $r(t)$. In each 60-second trial, the first and last 10 seconds were "ramp-up" and "ramp-down" phases, in which the designed signal oscillated at 0.45 Hz with modulation and was added to modulated sum of sines signal. The $10-50$ second was the "sum-of-sines" phase, in which the designed signal followed summation of sinusoids in equation 1. Details are in Materials and Methods Section 5.2.1.
(B) Time domain offline data in "sum-of-sines" phase (40 seconds) from one fish in closed-loop $k = 1.1$ case. Red: reference signal $r(t)$; Black thick: averaged refuge position $s(t)$ across $n = 5$ trials, Black thin: refuge position in each individual trial; Blue thick: averaged fish position $y(t)$ across $n = 5$ trials, Blue thin: fish position in each individual trial.

directly act on adjusting the nodal point position u. Thus, we have

$$\begin{aligned} m\ddot{x} + \beta\dot{x} &= \kappa(u + d_m) + F_t \\ &= \kappa u + (\kappa d_m + F_t) \\ &= \kappa u + F_d, \end{aligned} \tag{6}$$

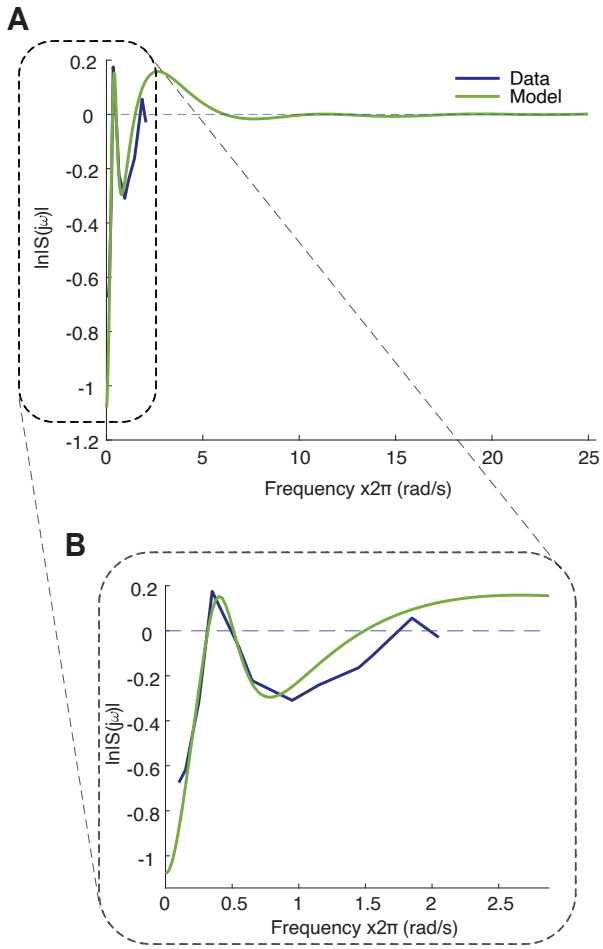

Figure S2. (A) Fitted sensitivity function in $k = 1.1$ case with model (see Supplemental Materials Section 8.1) from one fish (green) with frequency range of $0 - 2\pi \times 25$ rad/s and raw data (blue). A huge bump above zero indicates that the tuned controller of fish reduced sensitivity to low frequency disturbances (< 2.05 Hz) possibly as a cost of sacrificing the sensitivity to frequency band $2\pi \times 2 - 2\pi \times 5$ rad/s which is mostly out of our experimental design. (B) Zoomed version of (A) to the frequency range in our experiments.

Here, F_d is the combined "disturbance" from turbulence forces and motor command noise and does not impact the structure of the plant model.

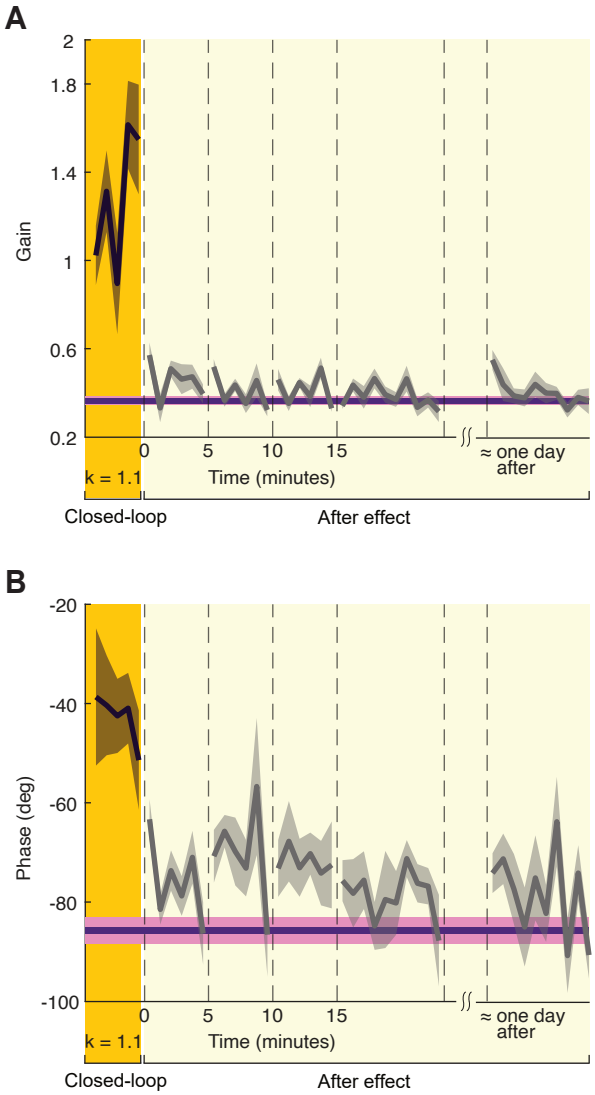

Figure S3. Fish FRF gain at 1.15 Hz(A) and phase at 0.65 Hz(B) from late learning "$k = 1.1$" (when $t < 0$), "just after," "5 minutes after," "10 minutes after," "15 minutes after," and "$\approx$ one day after" cases, by bootstrapping online data (10000 times) across $N = 6$ fish. The gray solid lines are mean and shaded regions are standard deviations (stds). The purple solid line is the mean of bootstrapped data in "baseline," while shaded region is std.

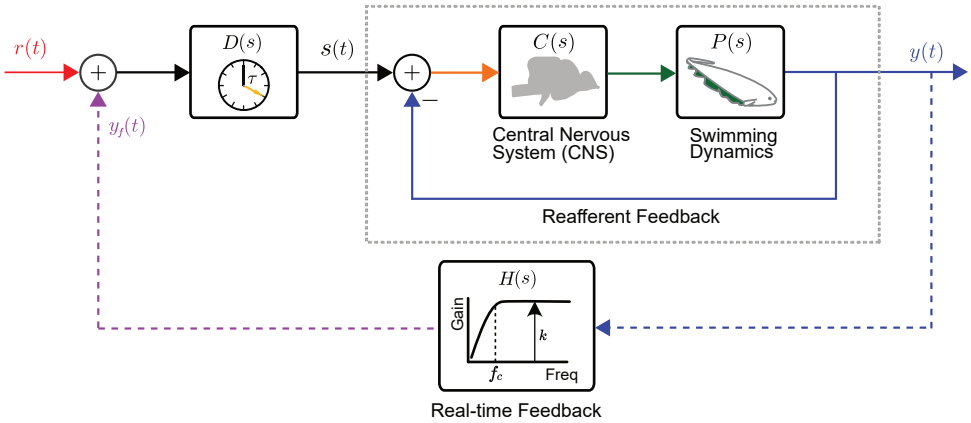

Figure S4. Block Diagram of the fish refuge tracking system with setup delay. The setup delay block $D(s)$ is at the forward loop. Identification of setup delay helped better estimate the sensitivity function.

References

[1] Hughes, G. The co-ordination of insect movements: II. the effect of limb amputation and the cutting of commissures in the cockroach (*Blatta oiuentalis*). *J Exp Biol* **34**, 306–333 (1957).

[2] Graham, D. The effect of amputation and leg restraint on the free walking coordination of the stick insect *Carausius morosus*. *J Comp Physiol* **116**, 91–116 (1977).

[3] Grabowska, M., Godlewska, E., Schmidt, J. & Daun-Gruhn, S. Quadrupedal gaits in hexapod animals–inter-leg coordination in free-walking adult stick insects. *J Exp Biol* **215**, 4255–4266 (2012).

[4] Owaki, D., Aonuma, H., Sugimoto, Y. & Ishiguro, A. Leg amputation modifies coordinated activation of the middle leg muscles in the cricket *Gryllus bimaculatus*. *Sci Rep* **11**, 1–12 (2021).

[5] Lockey, J. K. & Willis, M. A. One antenna, two antennae, big antennae, small: total antennae length, not bilateral symmetry, predicts odor-tracking performance in the american cockroach periplaneta americana. *J Exp Biol* **218**, 2156–2165 (2015).

[6] Dahake, A., Stöckl, A. L., Foster, J. J., Sane, S. P. & Kelber, A. The roles of vision and antennal mechanoreception in hawkmoth flight control. *eLife* **7**, e37606 (2018).

[7] Muijres, F. T., Iwasaki, N. A., Elzinga, M. J., Melis, J. M. & Dickinson, M. H. Flies compensate for unilateral wing damage through modular adjustments of wing and body kinematics. *Interface Focus* **7**, 20160103 (2017).

[8] Kihlström, K., Aiello, B., Warrant, E., Sponberg, S. & Stöckl, A. Wing damage affects flight kinematics but not flower tracking performance in hummingbird hawkmoths. *J Exp Biol* **224**, jeb236240 (2021).

[9] Salem, W. *et al.* Flies trade off stability and performance via adaptive compensation to wing damage. *Sci Adv* **8**, eabo0719 (2022).

[10] Krakauer, J. W., Hadjiosif, A. M., Xu, J., Wong, A. L. & Haith, A. M. Motor learning. *Compr Physiol* **9**, 613–663 (2019).

[11] Choi, J. T. & Bastian, A. J. Adaptation reveals independent control networks for human walking. *Nat Neurosci* **10**, 1055–1062 (2007).

[12] Finley, J. M., Long, A., Bastian, A. J. & Torres-Oviedo, G. Spatial and temporal control contribute to step length asymmetry during split-belt adaptation and hemiparetic gait. *Neurorehabil Neural Repair* **29**, 786–795 (2015).

[13] Telgen, S., Parvin, D. & Diedrichsen, J. Mirror reversal and visual rotation are learned and consolidated via separate mechanisms: recalibrating or learning *de novo*? *J Neurosci* **34**, 13768–13779 (2014).

[14] Yang, C. S., Cowan, N. J. & Haith, A. M. De novo learning versus adaptation of continuous control in a manual tracking task. *eLife* **10**, e62578 (2021).

[15] Lackner, J. R. & Dizio, P. Rapid adaptation to coriolis force perturbations of arm trajectory. *J Neurophysiol* **72**, 299–313 (1994).

[16] Nguyen, K. P. *et al.* The 24-h savings of adaptation to novel movement dynamics initially reflects the recall of previous performance. *J Neurophysiol* **122**, 933–946 (2019).

[17] Cowan, N. J. *et al.* Feedback control as a framework for understanding tradeoffs in biology. *Integr Comp Biol* **54**, 223–237 (2014).

[18] Cowan, N. J. & Fortune, E. S. The critical role of locomotion mechanics in decoding sensory systems. *J Neurosci* **27**, 1123–1128 (2007).

[19] Biswas, D. *et al.* Closed-loop control of active sensing movements regulates sensory slip. *Curr Biol* **28**, 4029–4036 (2018).

[20] Stamper, S. A., Roth, E., Cowan, N. J. & Fortune, E. S. Active sensing via movement shapes spatiotemporal patterns of sensory feedback. *J Exp Biol* **215**, 1567–1574 (2012).

[21] Chen, C., Murphey, T. D. & MacIver, M. A. Tuning movement for sensing in an uncertain world. *eLife* **9**, e52371 (2020).

[22] Rose, G. J. & Canfield, J. G. Longitudinal tracking responses of the weakly electric fish, sternopygus. *J Comp Physiol A* **171**, 791–798 (1993).

[23] Roth, E., Zhuang, K., Stamper, S. A., Fortune, E. S. & Cowan, N. J. Stimulus predictability mediates a switch in locomotor smooth pursuit performance for *Eigenmannia virescens*. *J Exp Biol* **214**, 1170–1180 (2011).

[24] Sefati, S. *et al.* Mutually opposing forces during locomotion can eliminate the tradeoff between maneuverability and stability. *Proc Natl Acad Sci U.S.A.* **110**, 18798–18803 (2013).

[25] Uyanik, I. *et al.* Variability in locomotor dynamics reveals the critical role of feedback in task control. *eLife* **9**, e51219 (2020).

[26] Yared, D. G. *Learning of Novel Dynamics in Eigenmannia virescens Refuge Tracking Task.* Master's thesis, Johns Hopkins University (2020).

[27] Åström, K. J. & Murray, R. M. Feedback systems. In *Feedback Systems* (Princeton university press, 2010).

[28] de C Hamilton, A. F., Jones, K. E. & Wolpert, D. M. The scaling of motor noise with muscle strength and motor unit number in humans. *Exp Brain Res* **157**, 417–430 (2004).

[29] Combes, S. A. & Dudley, R. Turbulence-driven instabilities limit insect flight performance. *Proc Natl Acad Sci U.S.A.* **106**, 9105–9108 (2009).

[30] Csete, M. E. & Doyle, J. C. Reverse engineering of biological complexity. *Science* **295**, 1664–1669 (2002).

[31] Crevecoeur, F., Scott, S. H. & Cluff, T. Robust control in human reaching movements: a model-free strategy to compensate for unpredictable disturbances. *J Neurosci* **39**, 8135–8148 (2019).

[32] Matthews, M. & Sponberg, S. Hawkmoth flight in the unsteady wakes of flowers. *J Exp Biol* **221**, jeb179259 (2018).

[33] Sponberg, S., Dyhr, J. P., Hall, R. W. & Daniel, T. L. Luminance-dependent visual processing enables moth flight in low light. *Science* **348**, 1245–1248 (2015).

[34] Kasuga, S., Telgen, S., Ushiba, J., Nozaki, D. & Diedrichsen, J. Learning feedback and feedforward control in a mirror-reversed visual environment. *J Neurophysiol* **114**, 2187–2193 (2015).

[35] Hitschfeld, É. M., Stamper, S. A., Vonderschen, K., Fortune, E. S. & Chacron, M. J. Effects of restraint and immobilization on electrosensory behaviors of weakly electric fish. *ILAR journal* **50**, 361–372 (2009).

[36] Mathis, A. *et al.* DeepLabCut: Markerless pose estimation of user-defined body parts with deep learning. *Nat Neurosci* **21**, 1281–1289 (2018).

[37] Yang, Y. *A Comparison of System Identification Techniques for Refuge Tracking Behavior in Eigenmannia virescens.* Master's thesis, Johns Hopkins University (2020).

[38] Costa-Castelló, R. & Dormido, S. An interactive tool to introduce the waterbed effect. *IFAC-PapersOnLine* **48**, 259–264 (2015).

[39] Stamper, S. A., Madhav, M. S., Cowan, N. J. & Fortune, E. S. Using control theory to characterize active sensing in weakly electric fishes. In *Electroreception: Fundamental Insights from Comparative Approaches*, 227–249 (Springer, 2019).